IOP PUBLISHING JOURNAL OF PHYSICS: CONDENSED MATTER

J. Phys.: Condens. Matter **20** (2008) 354009 (15pp) doi:10.1088/0953-8984/20/35/354009

# Elucidating atomic-scale friction using molecular dynamics and specialized analysis techniques

**Judith A Harrison[1,3], J David Schall[1], M Todd Knippenberg[1], Guangtu Gao[1] and Paul T Mikulski[2]**

[1] Department of Chemistry, United States Naval Academy, Annapolis, MD 21402, USA
[2] Department of Physics, United States Naval Academy, Annapolis, MD 21402, USA

E-mail: jah@usna.edu

Received 29 February 2008, in final form 5 May 2008
Published 11 August 2008
Online at stacks.iop.org/JPhysCM/20/354009

**Abstract**
Because all quantities associated with a given atom are known as a function of time, molecular dynamics simulations can provide unparalleled insight into dynamic processes. Many quantities calculated from simulations can be directly compared to experimental values, while others provide information not available from experiment. For example, the tilt and methyl angles of chains within a self-assembled monolayer and the amount of hydrogen in a diamond-like carbon (DLC) film are measurable in an experiment. In contrast, the atomic contact force on a single substrate atom, i.e., the force on that atom due to the tip atoms only, and the changes in hybridization of a carbon atom within a DLC film during sliding are not quantities that are currently obtainable from experiments. Herein, the computation of many quantities, including the ones discussed above, and the unique insights that they provided into compression, friction, and wear are discussed.

(Some figures in this article are in colour only in the electronic version)

## 1. Why classical molecular dynamics?

The basic setup of molecular dynamics (MD) algorithms is straightforward and has been discussed in a number of reviews [1–4]. In this technique, atoms are treated as discrete particles. The force on each atom is calculated after determining the system geometry, the positions and velocities of each atom, and the boundary conditions. In quantum mechanical methods, electronic degrees of freedom are included and calculations are based on solutions of Schrödinger's wave equations. The inclusion of electrons and the complexity of the solutions to Schrödinger's equation limits system sizes to tens to hundreds of atoms, depending on the level of theory. To obtain useful information for larger systems sizes, analytic approximations to the atomic potentials have been developed, which attempt to capture the underlying quantum mechanical principles. These potentials are parameterized to reproduce bond energies, force constants, bond lengths, bond angles, and elastic constants that were obtained from quantum mechanical calculations and experiments. The atomic forces needed to propagate atoms in time are calculated from the derivative of the interatomic potential energy function with respect to position. The use of these potentials in classical molecular dynamics simulations has proven to be very useful in simulating a wide range of phenomena.

Even with the use of classical empirical potentials, MD is limited to modeling systems comprised of tens to hundreds of thousands of atoms (more for parallel codes) and simulated times on the order of nanoseconds. Analogous experimental systems rarely, if ever, deal directly with measurements that only involve size and timescales to which MD is confined. Given this serious limitation, why is MD viewed as a useful tool?

The usefulness of MD lies in the wealth of atomic-scale information it provides, information that without question will long be unavailable from experiment. This atomic-scale information, if explored carefully and creatively, can

[3] Author to whom any correspondence should be addressed.

 © 2008 IOP Publishing Ltd Printed in the UK

provide a unique window into understanding properties that are measured experimentally. One could make an analogy with statistical mechanics where macroscopic system properties are elucidated by a consideration of system microstates even though experimentally one would never deal directly with microstates.

The wealth of atomic-scale information presents its own difficulties in that too much information is available. One of the largest concerns is how to manage, and 'sift through', all the information that is available, i.e., the positions, velocities, and forces on each atom at every simulation time step. Unfortunately, this is not an issue that needs to be addressed only during post-simulation analysis. It is simply not feasible to store all available information, and even if it were, it would not be practical to repeatedly process such a large data set when undertaking various analyses. Consequently, it is imperative to thoughtfully consider what information should be saved over the course of a simulation. With the duration of simulations often lasting weeks or months, rerunning simulations simply to get at information that was not originally written is frustrating, though sometimes necessary. Rarely can one anticipate a set of canned analyses that is completely satisfactory given that simulations are exploring systems that are not completely understood. Thus, the ideal is to write enough information such that the data set is flexible and manageable enough to allow for a variety of creative analysis types, including types of analyses that were not anticipated prior to running the simulations.

In what follows, some of the analysis techniques that we have employed in the course of our MD simulations are reviewed and the insights they have provided into our examinations of the mechanical and tribological properties of diamond-like carbon (DLC) films and self-assembled monolayers (SAMS) are discussed.

### *1.1. The importance of the potential*

Molecular dynamics simulations require some way to evaluate the forces between atoms. Ideally, atomic interactions would be calculated from first-principles calculations. However, such calculations are computationally intensive, increasing by orders of magnitude with an increase in the number of atoms. Therefore, to obtain useful information in a reasonable amount of time, researchers have developed empirical and semiempirical approximations to atomic potentials.

The choice of the potential energy function to be used in any simulation should be governed by careful consideration of the processes and materials to be modeled, and the level of detail one hopes to attain. Simple potentials, such as the Lennard-Jones (LJ), potential have been used extensively to model general behavior in rare-gas clusters [5], between polymer segments, and in tribological simulations [6, 7, 1, 8]. There are other simple potentials that make use of the LJ potential, such as the united-atom model [9] and the bead-spring model [10]. For metals, the embedded-atom method (EAM) has been highly successful and has opened up a range of phenomena to simulation [11–14].

A logical extension of the pair potential is to assume that the energy can be written as a many-body expansion of the relative positions of the atoms. Tersoff was the first to use this idea to incorporate the structural chemistry of covalently bonded systems into a potential energy function [15–18]. Using the Tersoff carbon potential as a model, Brenner developed an empirical bond-order expression that described covalent bonding in hydrocarbon molecules and solid-state carbon [19]. This so-called reactive empirical bond-order potential (REBO) was originally developed to model chemical vapor deposition of diamond films, though it is now widely used in simulating many other reactive processes and it has spawned potentials for other covalent interactions [20–22]. This hydrocarbon potential was recently revised [23] so that it provides a significantly better description of bond energies, bond lengths, force constants, elastic properties [24, 25], interstitial defect energies, and surface energies for diamond. Parameters within the second-generation REBO formalism [23] have recently been developed for C–O and O–H [26] interactions as well as Si–Si [27] interactions.

To model self-assembled monolayers it is necessary to include intermolecular forces between chains as well as intramolecular, or covalent, forces within the chains. The addition of long-range intermolecular forces to a potential that is capable of modeling short-range covalent bond breaking and bond forming must be carried out in a way that preserves the reactivity. For species that might form a bond if they were close enough to react, the long-range potential must be 'turned off'. Goddard and coworkers combined long-range forces with the second-generation REBO by using a distance-based switching function [28].

The adaptive intermolecular REBO (AIREBO) potential utilizes both distance-based ($S_{\text{distance}}$) and connectivity-based ($S_{\text{connectivity}}$) switching functions, as well as a hypothetical bond-order switch $S_{\text{bond}}$, to smoothly interpolate between pure bonded and pure nonbonded interactions [29, 30]. The LJ potential may be either completely or partially turned off in response to the chemical environment of an interacting pair. Each one of the three switching functions may turn off the LJ-interaction partially or entirely,

$$E^{\text{LJ}} = (1 - S_{\text{distance}} S_{\text{bond}})(1 - S_{\text{connectivity}}) V^{\text{LJ}}. \qquad (1)$$

For each of these switches, a value of 1 is associated with turning off the LJ-interaction completely, a value of 0 is associated with a full LJ-interaction, and values in between are associated with a partial LJ-interaction. A full LJ-interaction will be included for atom pairs that are not (1, 2), (1, 3), or (1, 4) neighbors and are *either* beyond the cutoff distance $r^{\text{LJ max}}$ *or* have a bond order below $b^{\text{min}}$. Harrison and coworkers have used the AIREBO potential to examine the mechanical and tribological properties of self-assembled monolayers (SAMs) composed of hydrocarbon chains [31–37, 30, 38, 39].

## 2. Quantification of structure and disorder

In addition to chemical reactions that may be initiated by sliding, when two materials are pressed into contact, adhesion and deformation of the materials are possible. With that in mind, in both experimental and simulated systems, care should

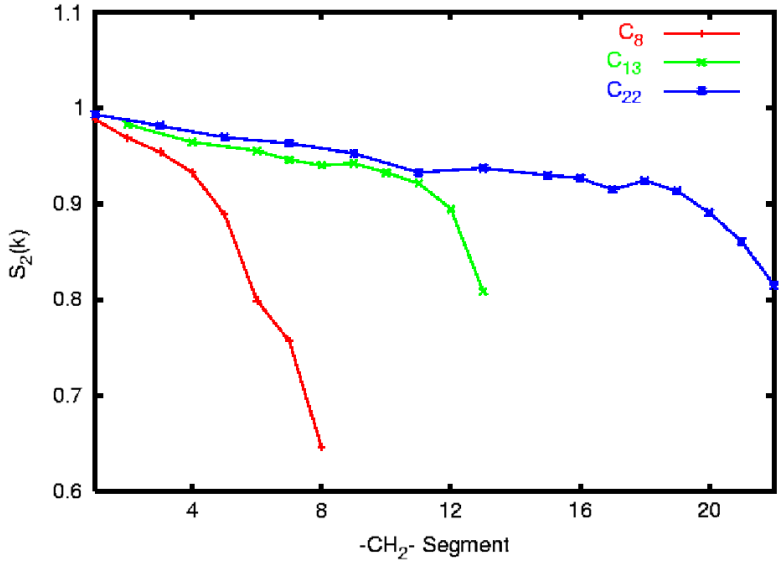


**Figure 1.** Two-dimensional structure factor $S_2$ as a function of chain segment (–$CH_2$– or –$CH_3$) for equilibrated $C_8$ (red line with pluses), $C_{13}$ (green line with crosses) and $C_{22}$ (blue line with asterisks) monolayers composed of alkane chains. Two sets of $\boldsymbol{\tau}_i$ values are needed to calculate $\mathbf{k}_i$. The first set of values was 5.028 and 0.0 Å and the second set was 2.513 and 4.356 Å. Adapted from [31].

be taken to quantify the state of the materials before, during, and after contact. One advantage of MD simulations over experiments is that the positions, forces, and velocities (along with higher order time derivatives) are known for all atoms, at all times, during the simulation. This allows for the calculation of many interesting quantities throughout the simulation that can lend significant insight into the essential physics being studied.

In our examinations of the indentation and friction of SAMs composed of hydrocarbon chains, several quantities have been used to quantify structural changes. These include tilt angle, methyl angle, azimuthal angle, torsional angles, and the two-dimensional structure factor. Self-assembled monolayers are composed of individual chains attached to a substrate. Several angles associated with individual chains can yield insight into the collective order of the monolayer. Because it is possible to measure several of these angles experimentally, distributions obtained from simulations can be compared to experimentally determined values. The *cant*, or tilt angle $\theta$, for an individual chain is the angle formed by the surface normal and the chain-axis vector. This angle is obtained from the relationship $\cos(\theta) = z/h$, where $z$ is the length of a hydrocarbon chain along its carbon–carbon backbone and $h$ is the height of the hydrocarbon chain above the diamond substrate. Conformational changes in the ends of the chains can be quantified by calculating the methyl angle, or the angle between the surface normal and the last carbon–carbon bond (–$CH_2$–$CH_3$) in each chain. The *cant* of the monolayer chains and the methyl angle can be obtained from He-scattering data [40] and using sum-frequency vibrational spectroscopy [41], respectively. It is also possible to calculate the intrachain dihedral angles along the chain backbone. The dihedral angle is defined in the usual way as the angle between $C_a$ and $C_d$ when a chain segment $C_a$–$C_b$–$C_c$–$C_d$ is viewed along the bond between $C_b$ and $C_c$. This angle is useful for identifying the formation of gauche-like defects along the chain backbone. Finally, the azimuthal angle [37] can be used to monitor the number of rotations the terminal groups of each chain undergo during sliding or indentation.

The two-dimensional (2D) structure factor, $S_\alpha$ is given by [31]

$$S_\alpha = \langle \cos \mathbf{k}_\alpha \cdot \mathbf{r}_{ij} \rangle \tag{2}$$

where the $\mathbf{k}_\alpha$ is a reciprocal lattice vector and $\mathbf{r}_{ij} = \mathbf{r}_i - \mathbf{r}_j$ is the vector between atoms $i$ and $j$. For a crystal with well-defined 2D symmetry translations, the reciprocal lattice vectors $\mathbf{k}_\alpha$ can be calculated from the primitive lattice translations $\boldsymbol{\tau}_1$ and $\boldsymbol{\tau}_2$ using

$$\mathbf{k}_1 = 2\pi \frac{\boldsymbol{\tau}_1 - \alpha_2 \boldsymbol{\tau}_2}{\boldsymbol{\tau}_1 \cdot (\boldsymbol{\tau}_1 - \alpha_2 \boldsymbol{\tau}_2)} \tag{3}$$

and

$$\mathbf{k}_2 = 2\pi \frac{\boldsymbol{\tau}_2 - \alpha_1 \boldsymbol{\tau}_1}{\boldsymbol{\tau}_2 \cdot (\boldsymbol{\tau}_2 - \alpha_1 \boldsymbol{\tau}_1)}, \tag{4}$$

where $\alpha_n = \frac{\boldsymbol{\tau}_1 \cdot \boldsymbol{\tau}_2}{\boldsymbol{\tau}_n \cdot \boldsymbol{\tau}_n}$. These definitions guarantee that $\mathbf{k}_i \cdot \boldsymbol{\tau}_j = \delta_{ij} 2\pi$. With these definitions, the 2D structure factor $S_\alpha$ will have a value of one if the system is translationally invariant under $\boldsymbol{\tau}_1$ and $\boldsymbol{\tau}_2$. Consequently, individual segments of a well-ordered SAM will have $S_\alpha$ values near one if the reciprocal lattice vectors are calculated based on the attachment sites to the substrate. The $S_\alpha$ values will decrease as the monolayer loses its translational order and will average near zero for a completely disordered system.

### *2.1. Effects of tip shape, compression, and sliding on disorder in SAMs*

Model SAMs can be constructed by attaching hydrocarbon chains to diamond substrates in regular patterns. Because SAMs composed of both alkanethiols and alkylsilanes contain hydrocarbon chains, such systems serve as model SAMs.

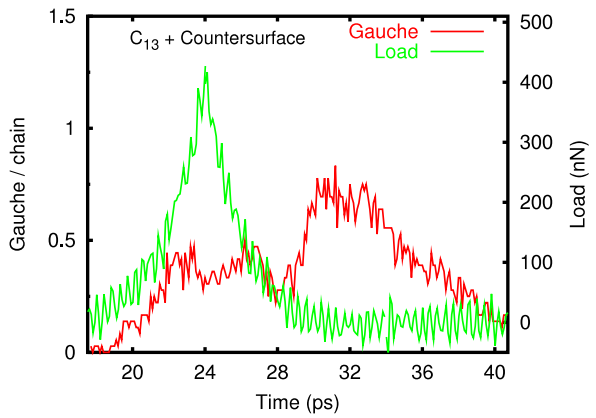


**Figure 2.** Number of gauche defects per chain (darker red line) within the monolayer and the load (lighter green line) as a function of simulation time for the compression (and relaxation) of a monolayer composed of $C_{13}$ alkane chains using a hydrogen-terminated diamond(111) (1 × 1)–H surface. The monolayer contained a total of 36 alkane chains. Adapted from [32].

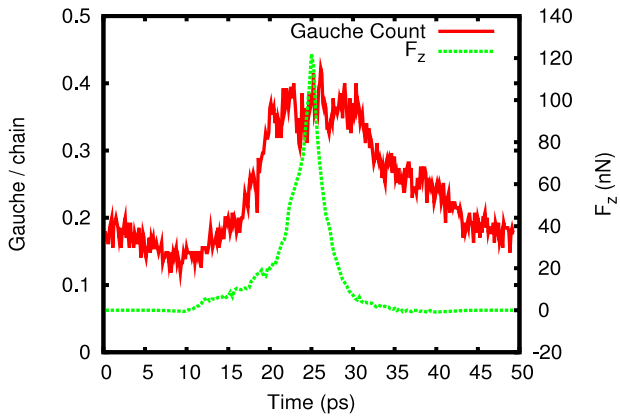


**Figure 3.** Number of gauche defects per chain (solid, dark red line) within the monolayer composed of $C_{14}$ alkane chains and the load ($F_z$) (dotted, light green line) as a function of simulation time for the compression and relaxation of a monolayer using a $C_{720}$ fullerene [42]. The system contained 270 chains and the plane that contained the monolayer was 75.4 Å by 78.4 Å.

Carbon nanotubes, diamond surfaces, amorphous carbon surfaces, and fullerenes have all been used as counterfaces to examine indentation and friction in these model SAMs systems [31–34, 36, 37, 35, 38, 39, 42].

Covalently bonding alkane chains to diamond (111) surfaces in the (2 × 2) arrangement yields approximately the same packing density and *cant* as alkanethiols on Au (111) [40] and serves as the ideal SAMs packing geometry. In the discussion that follows, the chains are attached to the diamond substrates with this packing unless otherwise specified. The 2D structure factor was used to quantify the order of model SAMs composed of $C_8$, $C_{13}$, and $C_{22}$ alkane chains (figure 1). These values were calculated for individual alkane chain segments (i.e., $–CH_2–$ and $–CH_3$) after equilibration of the monolayers at 300 K [31]. For a given monolayer, the values of $S_2$ revealed that carbon atoms in the chain segments of the monolayer were more ordered the closer they were to the diamond attachment site. Comparison of segments the same distance from the diamond substrate, but in different monolayers, showed that order in the monolayers increased as the chain length increased. This trend is also observed in alkylsilanes bound to mica [43]. The structure factor was also used to monitor the disruption of the translational ordering in SAMs during indentation by a capped, (10, 10) single-walled carbon nanotube (SWNT) [31]. The value of $S_2$ decreased upon indentation indicating a disruption in the monolayer's order. Retraction of the nanotube tip from a given monolayer allowed it to recover to an arrangement that was very close to its original lattice arrangement. In other words, the structure factors approached their pre-indentation values after retraction.

In addition to disrupting the translational ordering of the monolayer, indentation, compression, and sliding alter a number of other properties associated with the chains within the monolayer. Moreover, the degree of disruption depends on tip shape, tip size, and tip speed. For example, prior to indentation, the distribution of tilt angles of the chains within a monolayer composed of $C_{13}$ alkane chains is narrow and centered around 30° [32, 31]. Compression of the monolayer with an infinite diamond(111)(1×1)-H counterface [32] caused the peak in the tilt-angle distribution to shift to *larger* angles, while broadening only slightly. In other words, the chains moved away from the surface normal while largely maintaining their ordered structure. In contrast, using a finite-sized tip, such as a SWNT [32] or DWNT [30], to indent the monolayer caused the distribution of tilt angles to shift to *smaller* values and to broaden significantly. This shift was indicative of the chains within the monolayer 'standing up' straighter because the volume available to them decreased.

The penetration of finite-sized tips into the monolayer also introduces gauche-like defects within the individual monolayer chains. When all the intrachain dihedral angles are approximately 180°, the chains are defect free. If this angle is greater than 270° or less than 90°, gauche-like defects are present. Simulations have shown that the formation of these defects during indentation depends on the shape and size of the counterface [31, 32, 42] and upon the speed of indentation [30]. For example, when an infinitely flat diamond counterface was used to compress a monolayer composed of $C_{13}$ chains, the number of gauche defects increased with increasing load and reached a plateau (figure 2). This plateau corresponds to a conformation where the gauche defects are predominately located at the ends of all the chains. The additional application of load did not increase the number of defects because the volume available to the chains was reduced. Removing the load increases the volume available to the chains. Eventually, the chains will 'spring back' causing an increase in the number of gauche defects. After sufficient equilibration time in the absence of an applied load, these defects were removed from the monolayer.

Recently, a $C_{720}$ fullerene tip with a diameter of 26 Å was used as a probe tip to indent a monolayer composed of $C_{14}$ chains [42]. The finite contact area of the fullerene is smaller than the contact area of the infinite surface but larger than the rigid, SWNT nanotube used previously [31].

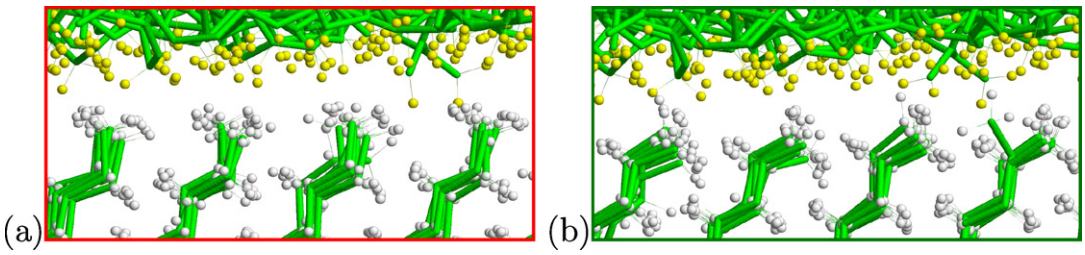


**Figure 4.** Close-up snapshots of the region near the sliding interface for the even ($C_{14}$ alkane chains) and odd ($C_{13}$ alkane chains) systems. The even and odd systems are composed of 100 $-(CH_2)_{13}CH_3$ and $-(CH_2)_{12}CH_3$ chains, respectively. Carbon bonds are shown in green wireframe, tip hydrogen atoms are shown as yellow spheres, and sample hydrogen atoms are shown as gray spheres. The hydrogenated, amorphous carbon tip contains 2803 atoms. (a) The odd number of carbon backbone atoms in the odd system results in the last carbon–carbon bond being oriented vertically. (b) The even number of carbon backbone atoms in the even system results in the last carbon–carbon bond being oriented horizontally. (Colour online.)

Due to its finite contact area, the fullerene tip is able to penetrate into the monolayer. The gauche defects for the indentation and retraction of the fullerene tip are shown in figure 3. In this case, the defects are formed all along the chain backbone on chains that are under, and adjacent to, the fullerene. The number of defects is approximately constant at the maximum load applied. In this case, the fullerene penetrated into the monolayer almost to the attachment point of the chains to the substrate. As a result, no new defects can be formed. Removing the fullerene from the monolayer allowed the defects to 'anneal' out. In both cases where a finite-sized tip was used to indent the monolayer [31, 42], the defects took longer to 'anneal' from the monolayer than when an infinite counterface was used. This is a natural result of the fact that the defects are farther down the chain backbone (farther from the interface) when finite-sized tips are used. Even small changes in the structure of the SAM-tip interface can have profound effects on the friction [37, 36, 33, 38, 39]. For example, recent simulations showed that a monolayer composed of $C_{13}$ alkane chains (odd system) generally had higher friction than a monolayer with identical packing but composed of $C_{14}$ alkane chains (even system) [37]. Because these monolayers differ in the orientation of the last carbon–carbon bond in the chain (figures 4(a) and (b)), examination of the methyl angle associated with ends of the chains ($-CH_2-CH_3$) is one way to quantify the structural changes present at the sliding interface. The probability distributions of methyl angles for the odd and even systems are shown in figure 5. These distributions were calculated during the course of the sliding simulations. At the lowest load, both distributions are centered about one angle, with the angle being approximately twice as large in the even system. In the even system, the application of load shifts the peak to slightly larger angles and broadens the distribution. In contrast, the application of a small amount of load to the odd system caused the first peak to broaden and resulted the emergence of a second peak near 100°. Thus, some of the terminal carbon–carbon bonds were shifted to a position that is nearly parallel to the substrate. This can also be thought of as a gauche defect in the end of the chain. The application of additional load caused the peak at lower methyl angles to decrease in intensity and to shift to higher angles. Eventually, this distribution becomes bimodal with peaks near 45° and 100°. At the highest load examined, over 60% of the chains were in the gauche conformation while only about 5% of the chains in the even system contained terminal gauche defects. The differences in the structure of the interface have a pronounced impact on friction. Friction in these two systems is discussed in detail in subsequent sections.

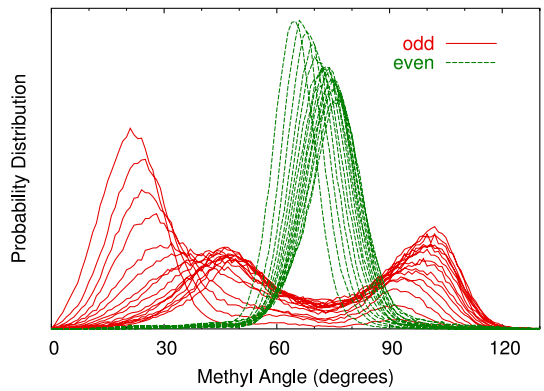


**Figure 5.** Probability distribution as a function of methyl angle. Green (dashed) and red (solid) lines correspond to a SAM composed of $C_{14}$ (even) and $C_{13}$ (odd) alkane chains, respectively. The series of lines of a given color represent different loads and more closely spaced lines within a color group represent moving to higher loads. The load range examined was 20 to 320 nN in 20 nN increments. Adapted from [37].

## 3. Contact forces: a tool for systems without wear

It is straightforward to develop a manageable, yet flexible, data set that facilitates a variety of post-simulation analyses for model non-wear tip–sample systems of the kind that are often explored in the context of tribology. In these types of systems, each atom is a member of either the set of tip or sample atoms with its membership being maintained throughout the course of the simulation. An atomic contact force for any atom can be defined as the vector sum of forces exerted on each atom due to interactions with the entire set of atoms of which it is not a member. For example, suppose that the $i$th atom is a sample

atom, the atomic contact force on this atom is then,

$$\mathbf{F}_i = \sum_{j}^{\substack{\text{tip}\\ \text{atoms}}} \mathbf{F}_{j\to i}. \tag{5}$$

It is important to note that this atomic contact force shows little connection to the net force on the atom because the force exerted by all other sample atoms is disregarded. Of course, it is the net force not the atomic contact force that is needed to evolve the atom's trajectory. Consequently, tracking the atomic contact force involves some modification to the simulation code so that every interaction between two atoms is assessed to determine if these atoms are from opposite sets. This is a distinction the MD code need not make to evolve atom trajectories. From an analysis point of view, the net force due to interaction with all other atoms is not particularly useful. In non-wear tribology simulations, net forces on individual atoms are usually quite small and must necessarily average very near zero if the velocity of the rigid layer is kept relatively constant. This is not to say that there is not much of interest going on, particularly for atoms near the interface between the tip and sample. At this interface, the net force on a sample atom may be quite small with the set of tip atoms exerting a large force on the sample atom and the remaining sample atoms largely canceling out this force.

There is one direct connection that can be made between net forces and atomic contact forces. That is, the net forces on the individual atoms of either set (tip or sample) summed vectorially give the same result as the vector sum of the atomic contact forces of either set with an overall difference in sign if comparing opposite sets. In other words, the net force exerted by the tip on the sample is equal and opposite to the net force exerted by sample on the tip, and these forces can be calculated by summing either net forces or atomic contact forces. This is simply a consequence of Newton's third law.

Truly atomistic simulations are computationally intensive because the time step must be chosen to be smaller than the timescale of the fastest physical system process. This is the vibration of bonded hydrogen atoms when hydrocarbons are being modeled and it requires a time step of only a fraction of a femtosecond. The timescale on which analysis is undertaken is orders of magnitude larger. Consequently, it is more manageable to track average atomic contact forces on individual atoms over a fixed number of simulation steps, $N$,

$$\overline{\mathbf{F}}_i = \frac{1}{N}\sum_{i}^{N}\left(\sum_{j}^{\substack{\text{tip}\\ \text{atoms}}} \mathbf{F}_{j\to i}\right). \tag{6}$$

In the work presented here, we expand upon our previously published work that has made extensive use of average atomic contact forces [36, 37]. All of these simulations have examined the friction of model SAMs composed of alkane chains, have utilized the AIREBO potential [29] with a time step in the range of 0.2–0.25 fs, and the atomic contact forces were averaged over sets of 2000 simulation steps. Hereafter, the term *average contact force* refers to the average atomic contact force. With this definition of average contact forces, all of the information available about the forces on each atom at every time step can be distilled down to a set of average force vectors (one force vector per particle) averaged over a timescale of interest. These force vectors can be summed to connect with a macroscopic property (i.e., the net force exerted by the sample on the tip) and can be analyzed individually to explore localized interactions between tip and sample at the sliding interface.

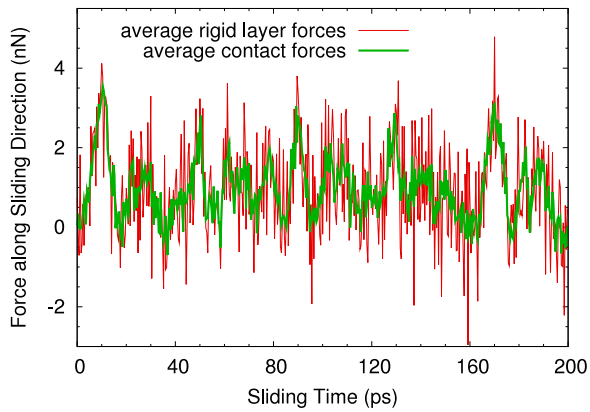


**Figure 6.** Net force along the sliding direction as a function of time on the set of rigid-tip atoms (thin line) and the entire set of tip atoms (thick line). The individual points from which the lines are constructed are averages over 2000 simulation steps or 0.4 ps of sliding time. The simulation system is composed of a monolayer of 100 $C_{14}$ alkane chains in contact with an amorphous carbon tip under 20 nN of load. The sliding direction is with the chain *cant*. (Other simulations details are given in the text.)

It is important to note that the quantity that is most directly connected with what is measured experimentally is the net force on the rigid-layer tip atoms, not the average contact force summed over all tip atoms (i.e., the net average contact force). In fact, the atomic contact forces on rigid-tip atoms and atoms near the rigid layer are completely negligible because they are far away from the sliding interface. Thus, it is important to establish that there is a high degree of correlation between the net force on rigid-layer tip atoms and the net average contact force exerted by the sample on the tip. Figure 6 shows the force along the sliding direction as a function of time for an amorphous hydrocarbon tip sliding against a SAM composed of $C_{14}$ alkane chains attached to diamond (111) in the ideal packing arrangement. The tip is sliding in the direction of chain *cant* and it is maintained at a constant load of 20 nN. Additional simulation details have been published previously [36, 37]. The curve showing large random looking fluctuations is the net force on the rigid-layer tip atoms, whereas the smoother curve shows the net average contact force on all tip atoms. It is very clear from this figure that the net force on the rigid atoms is highly correlated with the net average contact force on all tip atoms. Large random fluctuations of the net rigid-layer force are expected because the only atoms exerting appreciable forces on the rigid layer are covalently bonded to it. In contrast, atoms across the interface interact with the tip via LJ forces, which are much weaker than the widely and quickly varying covalent forces on rigid-layer atoms. This strong correlation between the net rigid-layer

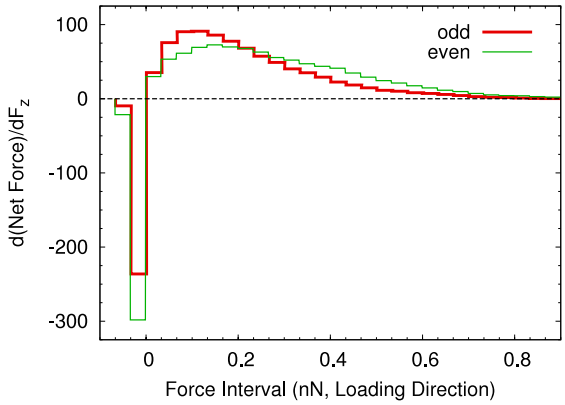


**Figure 7.** Loading-force distribution for sample atoms. The average $z$-component of force on each atom belonging to the sample (SAM and substrate) was examined over each time interval (averages are for each set of 2000 simulation steps). Each $z$-component force was added to its corresponding force interval bin. Each bin was then divided by the total number of time intervals and the bin width. Thus, integrating over the curve gives the average system load. The negative and positive sides of the distribution correspond to attracting and repelling forces, respectively. Larger peaks correspond to a larger number of atoms added to that force interval. The load on the amorphous carbon tip was maintained at 20 nN and the sliding direction is with the chain *cant*. (Other simulations details are given in the text.)

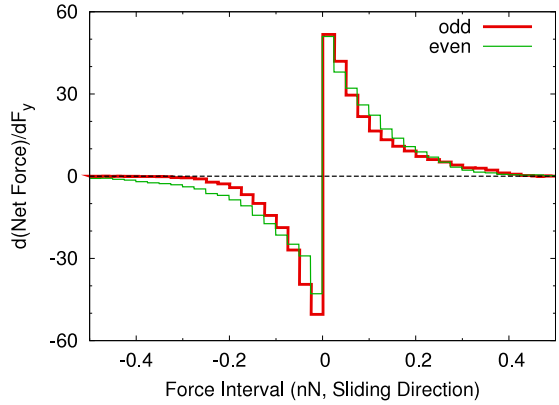


**Figure 8.** Sliding-direction force distribution for sample atoms. The average $y$-component of force on each atom belonging to the sample (SAM and substrate) was examined over each time interval (averages are for each set of 2000 simulation steps). Each $y$-component of force was added to its corresponding force interval bin. Each bin was then divided by the total number of time intervals and the bin width. Thus, integrating over the curve gives the average system friction. The negative and positive sides of the distribution correspond to pushing and resisting forces, respectively. (Other simulation details are given in the text.)

forces and the net average contact forces is generally present in all non-wear, tip–sample tribology simulations where periodic boundary conditions are used to model a very large contact area. Averaging over time to calculate friction versus load shows virtually no meaningful difference between the friction calculated from the rigid layer alone and from the full set of tip atoms. Consequently, analysis of average contact forces, instead of rigid-layer forces, can be undertaken with confidence.

### *3.1. Contact-force distributions*

A primary goal of an analysis of average contact forces is to find correlations between trends in average contact forces and specific structural features of the tip and sample over a range of target sliding loads. It can be useful, however, before searching for such connections, to get a general feel for what warrants closer study by examining contact-forces distributions. For instance, while it may be known that the total load is about 20 nN, is this load carried primarily by a few atoms at the sliding interface, or is the load spread more uniformly across most of the atoms at the sliding interface? Given a lack of experience with this kind of detail, it is helpful if these questions are asked in the context of a comparison between systems that are very similar, though different in some essential way. The tactic of relative comparisons is all the more important when considering the limitations of molecular dynamics in its ability to directly connect with experimental systems.

Figures 7 and 8 show average contact-force distributions along the loading and sliding directions when a hydrogenated amorphous carbon tip is in contact with the even and odd systems. More important than the overall length of the chains in these alkane SAMs is the orientation of the ends of the chains (–$CH_2$–$CH_3$) near the sliding interface. Figures 4(a) and (b) show close-ups of these systems at the sliding interface while under the 20 nN target load. The orientation of the chains is determined by whether the total number of carbon atoms in the chain backbone is even or odd and is also apparent from an examination of the methyl angle of the chains (figure 5). The average contact-force histograms of figures 7 and 8 examine the average contact forces for the set of sample atoms. The contact forces averaged over each 0.4 ps interval (2000 simulation steps) were analyzed for each atom that makes up the SAM and diamond substrate. Each force component falls within one of the histogram bins and that bin is updated by adding in the force contribution from that atom. The reason for adding forces to histogram bins rather than tracking a count is twofold. First, it focuses attention on those atoms that are the large contributors to the net force on the tip, while a count would focus the histogram almost entirely on the lowest force bins where there are many atoms contributing very small forces. Second, by dividing each bin by the total number of time intervals and also by the width of the bin, the integral over these histograms gives the load and friction for the run. After steady-state sliding was established at the target load, data was binned for two passes over the sample (400 ps).

The negative side of figure 7 corresponds to atoms that are in attractive contact with the tip. Because these attractive forces are weak LJ forces, all contributions appear in the two lowest force bins. The odd system is more strongly peaked at low repulsive force bins and shows less contributing atoms to the larger repulsive force bins than the even system. Thus, there are a larger number of atoms supporting the load and, on average, each one carries a smaller fraction of the load. A count of the average number of atoms in repulsive contact for

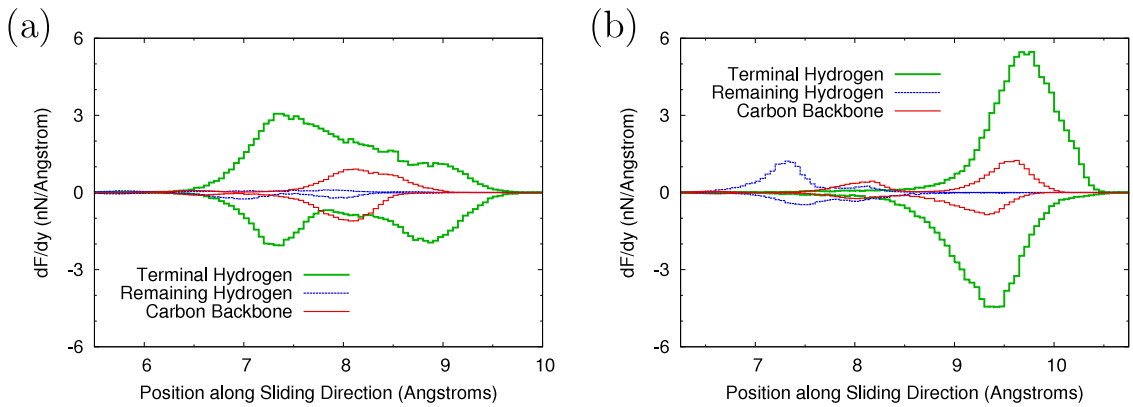


**Figure 9.** Histograms of average contact forces along the sliding direction for the odd (a) and even (b) systems. Binning is according to the location of each contributing atom from the SAM along the sliding direction. Resisting (positive) and pushing (negative) force histograms were tracked. The $y$-positions of the atoms belonging to each chain have been translated such that the substrate atom to which each SAM chain is bound is taken to be $y = 0$. In effect, all SAM chains have been superimposed onto one another. The contributions from the carbon backbones of chains, the three terminal hydrogen atoms from each chain, and the non-terminal hydrogen atoms (only the two hydrogen atoms from the group below the terminal group are major contributors), are tracked as separate sets of atoms. The average contact-force distributions are substantial for only large positive values of $y$ with the maximum value of $y$ corresponding to the length of a chain when projected onto the $+y$ axis. (Colour online.)

these systems verifies this fact. The average number of atoms in repulsive contact is 265.9 and 232.8 in the odd and even systems, respectively. The snapshots in figures 4(a) and (b) show qualitatively why this is the case. The orientation of terminal groups places all three terminating hydrogen atoms close to the surface in the odd system. In contrast, the orientation of the terminal group for the even system buries one of the three terminal hydrogen atoms just below the sliding interface.

As load is increased, these structural features evolve in response to the compression of the SAMs affecting a change in the shape of the loading-force distribution. Differences in how the loading-force distribution changes correlate with differences in how the odd and even systems respond to compression. These structural differences were apparent in the methyl-angle distribution (figure 5). In the odd system, the more vertical carbon–carbon bond fell to the side (in the transverse direction) in response to a load. The result is that some of the terminal hydrogen atoms get buried just beneath the SAM surface. The additional canting of the chains exposes hydrogen atoms from the second group to the surface [37]. In contrast, the even system responds only by canting further, which brings the hydrogen atoms from the group below the terminal atom into more frequent repulsive contact. These mechanisms result in these systems becoming more alike with regard to the shapes of loading-force distributions and average number of atoms in repulsive contact as the load is increased. At 160 nN load, the average number of atoms in repulsive contact is 517.4 and 494.9 for the odd and even systems, respectively.

The 20 nN loads exhibits a trend of individual surface atoms carrying larger repelling forces partly because the even system must sustain a larger repelling force overall. This is due to the fact that the chain group below the terminal group ($-CH_2-$) lies closer to the sliding interface in the even system compared to the odd system, thus generating a larger overall attractive force. Because of the larger attractive forces present in the even system, the overall repelling force for the even system must also be larger than the odd system at the same load. This can be clearly seen by separately integrating over the negative and positive sides of the distribution. The load can then be expressed as the sum of a repelling force and an attracting force,

$$20.05\ \text{nN} = 28.25\ \text{nN} - 8.19\ \text{nN} \qquad \text{(loading, odd system)}. \tag{7}$$

$$20.08\ \text{nN} = 30.74\ \text{nN} - 10.66\ \text{nN} \qquad \text{(loading, even system)}. \tag{8}$$

The effect of this larger scale repelling force shifts the shape of the distribution to favor larger individual atom loading forces.

In figure 8, the positive side of the histogram corresponds to individual SAM atoms exerting forces that oppose the motion of the tip (resisting forces), while the negative side corresponds to individual SAM atoms that exert forces on the tip in the sliding direction (pushing forces). As a load baring atom slides over a single SAM chain, chain atoms ahead of the tip atom exert resisting forces and those that have cleared the tip atom exert pushing forces. In all SAM systems with the ideal packing geometry, there is a fairly high level of symmetry between the resisting and pushing sides of this distribution. Because friction is the integral over this histogram, it can be thought of as an asymmetry between the resisting and pushing sides of this histogram.

On the resisting side, the even and odd system are fairly similar, though overall it appears that the even system resists the tip slightly more with a favoring of more atoms at moderate resisting forces in the range of 0.05–0.25 nN. The larger resisting force in the odd system in the 0.025–0.050 nN bin accounts for a sizeable number of atoms because it takes more atoms to generate a large net resisting force in the small force bins.

The negative side of the histogram gives a more vivid contrast between the systems. The odd system has a higher

fraction of atoms that are only capable of generating small pushing forces. Counting the number of atoms that are both in repulsive (loading) and pushing contact shows the odd system has a higher number of these atoms (128.6 on average compared to 105.5 in the even system). However, the average pushing force per atom when in repelling and pushing contact is −0.0312 and −0.441 nN and for the odd and even systems, respectively. Integrating over the positive and negative sides of the histogram (figure 8), gives a total friction of 1.24 and 0.903 nN for the odd and even systems, respectively.

$$1.24\ \text{nN} = 5.70\ \text{nN} - 4.46\ \text{nN} \qquad \text{(friction, odd system)}, \tag{9}$$

$$0.90\ \text{nN} = 6.08\ \text{nN} - 5.18\ \text{nN} \qquad \text{(friction, even system)}. \tag{10}$$

## 4. Connecting structural features with contact forces

The trends revealed in the average contact-force histograms discussed above can be connected to structural features of the SAM. An example of such an analysis is presented below. Figures 9(a) and (b) show histograms of average contact forces along the sliding direction. There is a very dramatic contrast between the even and odd systems in these histograms owing to the orientation of the last carbon–carbon bond in the SAM chain. In the odd system, this bond is nearly vertical resulting in all three terminal hydrogen atoms taking on substantial fractions of the load. The pushing distribution for terminal hydrogen atoms does not appear shifted to a large extent relative to the resisting distribution. However, the shape of the pushing distribution is very different from the resisting distribution. For the even system, the terminal hydrogen distributions are quite a bit larger in scale and show an obvious shift between resisting and pushing forces with the peak of the resisting distribution shifted approximately one third of an angstrom in the positive-$y$ direction. One interpretation might be to consider these two quantities are dependent. The even system can sustain the higher resistive forces that tend to stretch these chains out a bit more along the sliding direction. This may be due to the terminal hydrogen atom that is buried just beneath the surface acting as a counter-lever to the average contact forces exerted on the two surface terminal hydrogen atoms. When all three terminal hydrogen atoms at the surface, there is much rotation of these terminal hydrogen atoms about the roughly vertical axis that passes through the parent terminal carbon atom [37]. Consequently, large resistive forces simply cannot be sustained in the odd system and apparently some of the terminal hydrogen atoms can barely respond at all with pushing forces.

A more likely interpretation for the strong peaks observed in the terminal hydrogen, contact-force distributions for the even system is that this system has a higher fraction of the chains within the SAM sharing nearly identical geometries. Thus, stronger peaks in the hydrogen atom distributions result. This more uniform geometry could also be closely associated with the hydrogen atom buried beneath the surface in that it is likely much more difficult to initiate rotations of the fixed structure of the three terminal hydrogen atoms about the axis defined by the last carbon–carbon bond of the chain. This ensures that chains keep a fairly tight, fixed structure. A comparison of the frequency of such rotations in the even and odd systems shows that these rotations are, in fact, much more frequent in the odd system [37], and that the frequency of such rotations correlates strongly with the subtle variation in frictional properties of these systems over loads in the range of 20–320 nN. This suggests that the peaks in the odd system are not as strong due to the fact that there is greater variety in the geometries of the terminal group. This tends to 'smear-out' the average contact-force distributions.

This example is only a single illustration of an analysis that connects average contact forces with structural features. There are a number of possible approaches to making such connections. Often reflecting on these analyses suggests complementary and/or more detailed investigations. The potential for such creative exploration is possible due to the nature of the atomic contact-force data set, which gives flexible and direct information about the local atomic-scale forces between tip and sample at the sliding interface. The regular and stable structure of self-assembled monolayers greatly aids in being able to clearly extract trends and correlations, as the technique of superposition of chains in the above example demonstrates. It is also seen in the above example that making the step from establishing a correlation to suggesting a physical interpretation can be tricky, and it is important to be able to support any possible interpretation with distinctly different types of analysis.

## 5. Indentation- and sliding-induced chemical reactions

The analysis techniques discussed above relied on the fact that chemical reactions were not initiated by sliding. The analysis of non-reactive systems was simplified by the fact that the neighbors of a given atom did not change as a function of time. Therefore, the location of any given atom can be 'tagged' at the start of the simulation and need not be tracked as the simulation proceeds. This is not the case if chemical reactions occur during the course of the simulation. One useful quantity that can be used for visually and quantitatively tracking chemical changes is the coordination number. This is simply the number of first-nearest neighbors of a single atom. Coordination number can be determined using either an arbitrary radial cutoff distance, such as an average between first- and second-neighbor distances, or by using a cutoff function as in equation (11).

$$C_{\text{i}} = \sum_{j \neq i}^{\substack{\text{all}\\ \text{atoms}}} f_{ij}^{\text{c}} \tag{11}$$

$$C_{\text{ave}} = \frac{1}{N} \sum_{i} C_{\text{i}}. \tag{12}$$

In the REBO hydrocarbon potential [23], the cutoff function, $f_{ij}^{\text{c}}$, is a continuous piecewise function of radial distance from atom $i$, which varies smoothly between one and zero, for atoms within and outside the interaction range of the

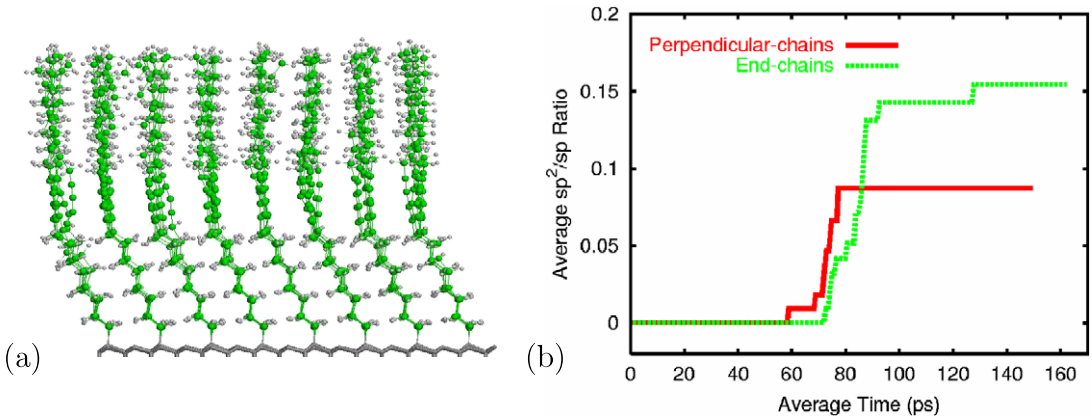


**Figure 10.** (a) The perpendicular-chain system prior to compression at 300 K. (The tip has been omitted for clarity.) The system contains 56 chains with the formula $–C_8H_{16}–C{\equiv}C–C{\equiv}C–C_8H_{17}$. Green and light gray spheres represent carbon and hydrogen atoms, respectively. The chains are attached to a diamond (111) substrate (shown in dark gray) in the (2 × 2) arrangement. Further simulation details can be found in [35]. (b) The ratio of $sp^2$-to-sp carbon as a function of time for the compression of two monolayers with the same number of atoms but with the diacetylene moieties in different locations within the chains. (Colour online.)

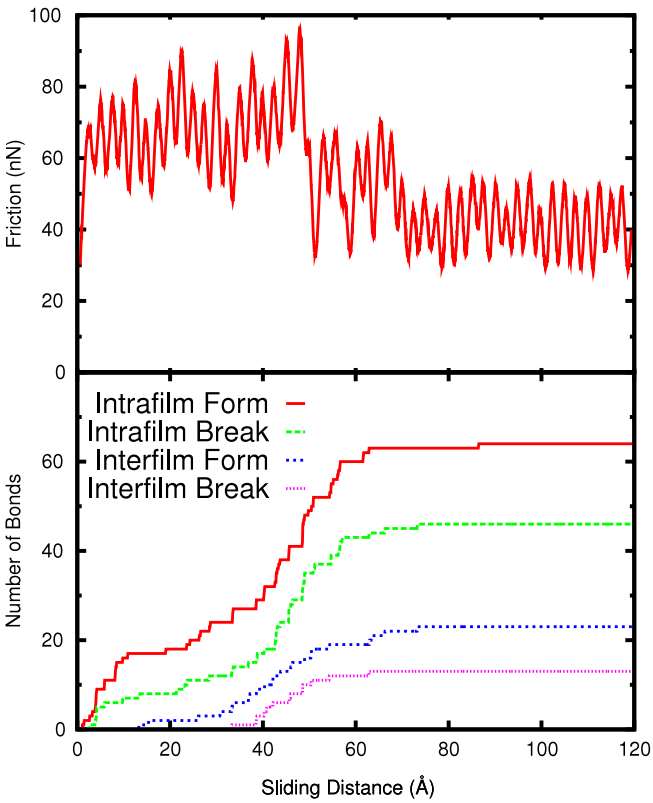


**Figure 11.** Friction versus sliding distance (upper panel) when a diamond(111)(1 × 1)-H counterface is in sliding contact with an amorphous carbon film under an average load is 300 nN. The friction is the force in the sliding direction on the counterface rigid layers averaged over 1.25 ps intervals. The sliding interface is 12 unit cells of diamond(111) in the sliding direction and 6 unit cells transverse to the sliding direction. The number of bonds broken and formed during sliding is shown in the lower panel. The labels intrafilm (top two lines) and interfilm (bottom two lines) correspond to bonds to within the amorphous carbon film and between the film and the diamond counterface, respectively. Other simulation details can be found in [61].

potential, respectively. The benefit of using the cutoff function defined in the potential is that it is capable of tracking partial neighbors as chemical reactions proceed. The coordination number of individual atoms ($C_i$), or average coordination number ($C_{ave}$) can be calculated at intervals throughout the simulation to track chemical changes.

The coordination number is a useful first approximation for the identification of the hybridization state of a given atom. For instance, $sp^3$-hybridized carbon corresponds to a coordination number of four, $sp^2$-hybridized carbon has a coordination of three, and sp-hybridized carbon has a coordination number of two. Due to the possible existence of carbon radicals, it is not possible to state definitively whether or not an atom truly has $sp^3$-hybridization or $sp^2$-hybridization without also considering the bond angles between adjacent atoms. Care must also be taken when interpreting the coordination number during the course of a simulation. For example, an $sp^3$-hybridized carbon atom has four neighbors, which may be carbon or hydrogen atoms. A chemical reaction could result in a change in the identity of these atoms without a change in hybridization. In other words, a careful analysis of the number of neighbors, the bond angles, and the identity of the neighbors of a given atom must be undertaken to definitively determine if chemical reactions have occurred during the course of a simulation. In what follows, several examples of MD simulations where the analysis of chemical reactions has been important are discussed.

### *5.1. Polymerization in SAMs*

Due to their potential use as molecular sensors [44, 45], the properties of SAMs containing chains with diacetylene moieties have been studied extensively [46, 47, 40]. For instance, the atomic-scale friction of unpolymerized diacetylene and polymerized monolayers has been examined using AFM [46, 48]. The compression and friction of model SAMs composed of chains containing diacetylene moieties was also examined using MD [35]. The simulations utilized the AIREBO potential [29] so that cross-linking, or polymerization, of the chains during the compression or sliding was possible. In that work, an irregular amorphous carbon counterface was brought into contact with three monolayers,

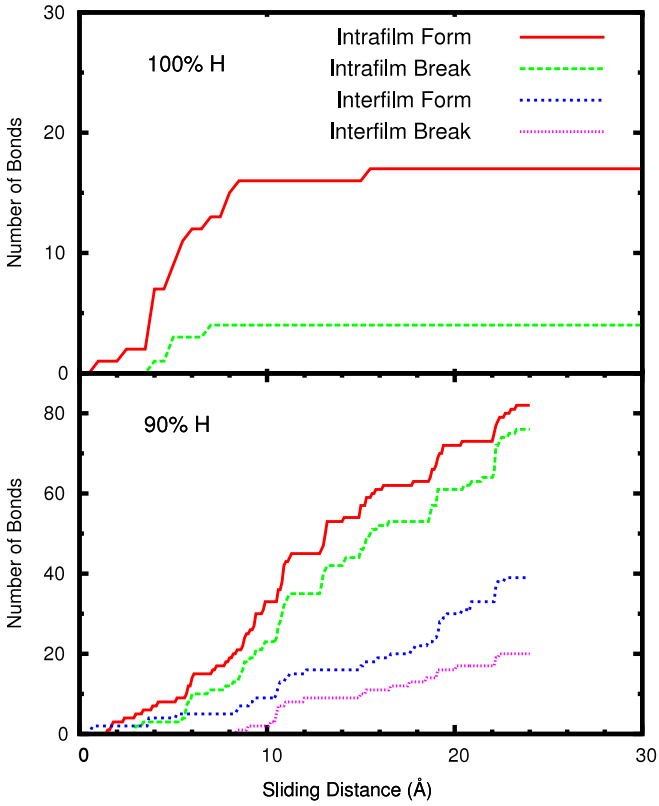


**Figure 12.** The number of bonds broken and formed during sliding. The terms in the legend are defined in figure 11. The data in the upper (lower) panel correspond to a simulation where the diamond counterface is 100% (90%) hydrogen terminated and has a load of 255 nN (240 nN). In the simulation depicted in the upper panel, no interfilm reactions occurred. In the lower panel, the intrafilm and interfilm reactions are the top two and the bottom two lines, respectively. The simulation systems are outlined in [61].

which differed only in location of the diacetylene moieties within the chains. The diacetylene moieties were located on the ends of the chains or in the middle of the chains. One such configuration, referred to as the perpendicular-chain system, is shown in figure 10(a). Varying the location of the sp-hybridized carbon allowed for the effects of its location on polymerization and friction to be examined.

The number of sp- and $sp^2$-hybridized carbon atoms was calculated during compression, and sliding, to monitor the creation of cross-links, i.e., $sp^2$-hybridization, between chains. Figure 10(b) shows the $sp^2$-to-sp carbon ratio as a function of time for the compression (and release) of the perpendicular-chain monolayer and a monolayer with the diacetylene moieties on the ends of the chains. These data show that the mechanical deformation of the monolayers initiates cross-linking between chains at the location of the diacetylene moieties. In addition, the degree of polymerization depends upon the location of the sp-hybridized regions within the chains. When the diacetylene moieties are on the ends of the chains, there is a greater degree of cross-linking occurs and chemical reactions with the amorphous carbon counterface occur. Cross-linking also occurs during shearing for all the monolayers examined. Altering the placement of the diacetylene moieties, even by one carbon atom within the chain, i.e., changing the spacer length, led to different polymerization patterns within the monolayers during sliding [35].

### *5.2. Diamond-like carbon: run-in and transfer layers*

Hydrogenated and non-hydrogenated metastable amorphous carbon materials (diamond-like carbon) and micro- and nanostructured diamond have a wide range of mechanical and tribological properties. For diamond-like carbon, these properties can depend on three-dimensional structure, $sp^3$-to-$sp^2$ ratios, hydrogen content, and deposition technique [49]. The grain size and roughness are additional variables that must be considered when dealing with microcrystalline and nanocrystalline diamond. The aforementioned carbon materials have been the focus of many experimental and theoretical studies due to their potential use as solid lubricants [49–54]. These types of coatings may prove useful

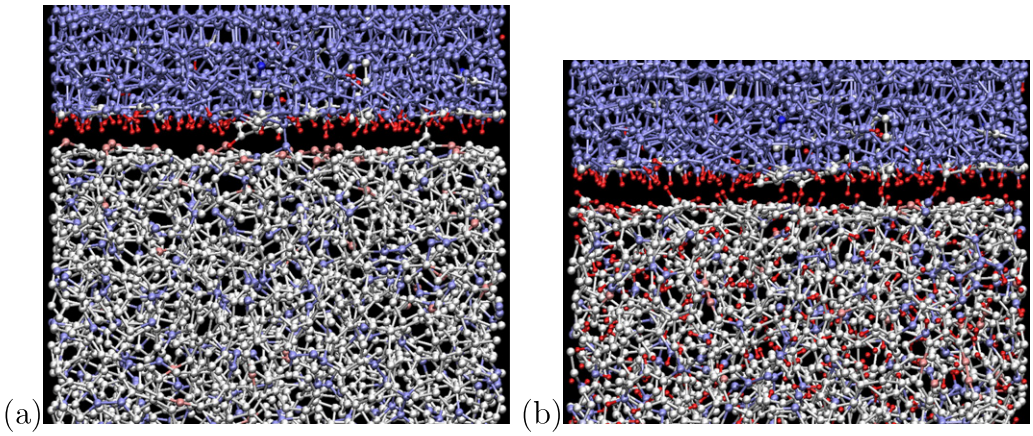


**Figure 13.** DLC counterfaces in contact with the $P_{00}$ and $P_{20}$ films in (a) and (b), respectively. The counterface has been used in several other studies where it is referred to as film IV [62, 4, 39]. The computational cell is approximately 30.2 Å by 26.1 Å in the sliding plane or 12 diamond(111) unit cells in the sliding direction and 6 unit cells transverse to the sliding direction. Large and small spheres represent carbon and hydrogen atoms, respectively. Carbon atoms are colored by coordination number. Large blue, gray, and red spheres correspond to $sp^3$-, $sp^2$-, and sp-hybridized atoms, respectively.

**Table 1.** Film composition and properties.

| Film | Total C | sp (%) | $sp^2$ (%) | $sp^3$ (%) | Total H | $c_{zz}$ (GPa) | Density (g $cm^{-3}$) |
|---|---|---|---|---|---|---|---|
| $P_{00}$ | 3000 | 2.2 | 85.3 | 12.5 | 0 | 358.7 | 2.75 |
| $P_{20}$ | 3000 | 2.1 | 83.4 | 14.5 | 750 | 295.4 | 2.40 |
| Counterface | 1115 | 0 | 5.6 | 94.4 | 120 | 462 | 2.86 |

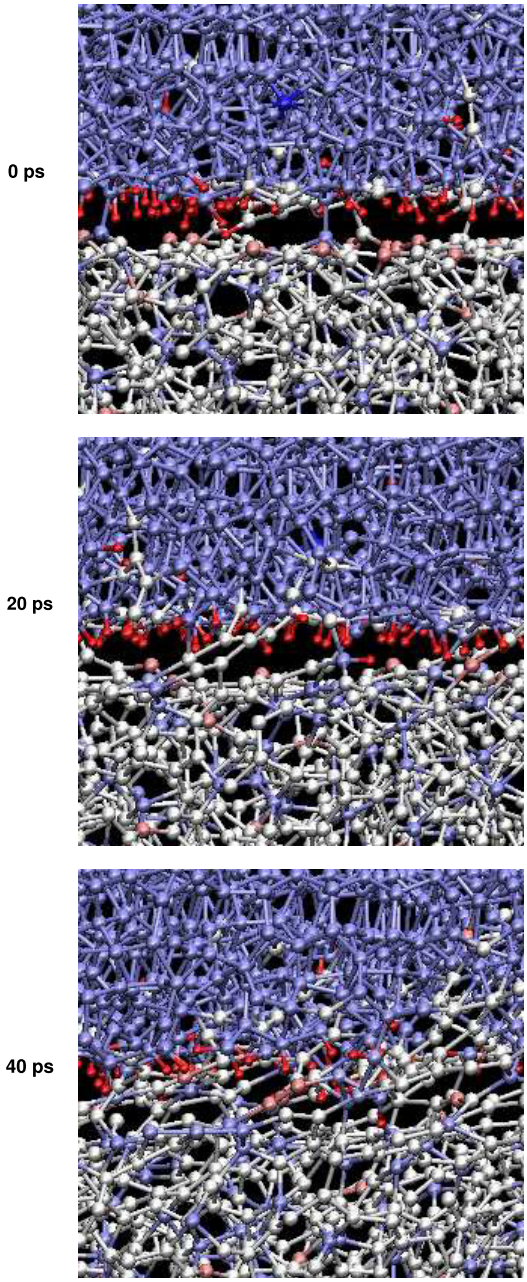


**Figure 14.** Snapshots from the simulation of a DLC counterface in sliding contact with the $P_{00}$ film. Large and small spheres represent carbon and hydrogen atoms, respectively. Carbon atoms are colored by coordination number. Large blue, gray, and red spheres correspond to $sp^3$-, $sp^2$-, and sp-hybridized atoms, respectively. The direction of counterface motion is from left to right.

in a number of applications, such as computer hard disks, microelectromechanical systems (MEMS), and space-based technologies [55–57].

Both microcrystalline and nanocrystalline diamond can exhibit a period of high friction, or 'run-in', when rubbing starts [58, 59] and recent AFM experiments suggest that 'run-in' also occurs at the nanoscale [60]. Continued rubbing typically leads to wear and reduced friction. We have used MD simulations to examine the friction and wear of a broad range of diamond and amorphous carbon coatings. One of these studies has lent insight into atomic-scale 'run-in' [61]. In that work, a hydrogen-terminated diamond(111) surface was placed in sliding contact with a DLC carbon film attached to a diamond substrate and the friction as a function of load was examined. The DLC film contained 1000 carbon atoms with 14.6%, 72.1%, and 13.3% of these atoms having $sp^3$-, $sp^2$-, and sp-hybridization, respectively. Additional simulation details have been published previously [61]. The friction versus sliding-distance data shown in the upper panel figure 11 were obtained at an average load of 300 nN. It is clear from these data that the friction decreases dramatically after approximately 50 Å of sliding. Insight into this reduction in friction was gained from examination of the data in the lower panel of figure 11. In this plot, the number of bonds broken and formed during sliding within the amorphous carbon film (intrafilm) and between the film and the diamond counterface (interfilm) are shown. Sliding caused many chemical changes within the film and some reactions between the film and the substrate. The chemical reactions ceased shortly after the reduction in friction occurred. Analysis of the number of bonds oriented in the sliding direction revealed that the film underwent a marked restructuring between 40 and 60 Å of sliding. In fact, a plot of the number of bonds oriented in the sliding direction versus sliding distance is nearly identical to the shape of the friction versus sliding-distance data [61].

Altering the nature of the counterface can dramatically influence the friction. Randomly removing hydrogen atoms from the diamond counterface caused an increase in the friction [61]. An examination of the number of bonds broken and formed during sliding reveals insight into the friction increase. Figure 12 shows the number of bonds formed and broken when an amorphous carbon film is in sliding contact with two different counterfaces, one with 100% and the second with 90% hydrogen termination. The removal of hydrogen from the counterface allows for the formation of bonds between the counterface and the film during sliding. The sliding motion eventually causes these bonds to break. In the absence of full hydrogen termination, the number of intrafilm bonds being broken and formed increases monotonically during sliding. In contrast, when the counterface was fully saturated, the number of intrafilm reactions increased slightly when sliding began but eventually reached a constant level. The larger number of chemical bonds between the substrate and the counterface caused the friction in the case of partial

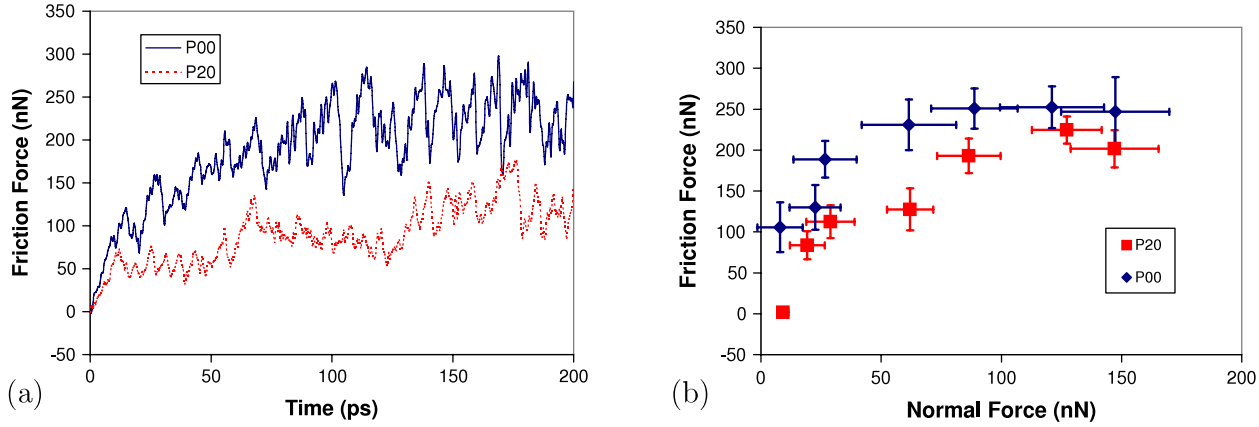


**Figure 15.** (a) Friction force on the rigid layer of the counterface when it is in sliding contact with the $P_{00}$ and $P_{20}$ films. The load on the counterface is maintained at 60 nN. (b) Average friction force as a function of load.

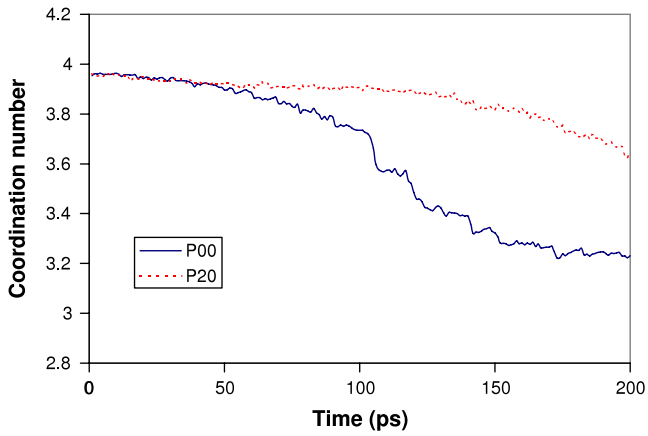


**Figure 16.** $C_{ave}$ of the counterface versus time when it is in sliding contact with the $P_{00}$ (solid blue line) and the $P_{20}$ (dashed red line) films under 60 nN of load. Data calculated from a 5 Å thick region that begins 5 Å from the interface to minimize the effects of counterface-film mixing.

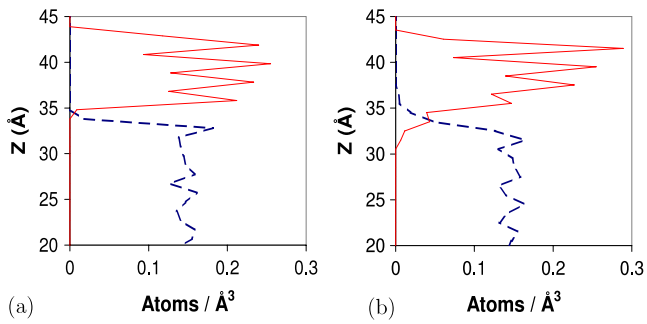


**Figure 17.** (a) Shown in the left panel is the density of carbon atoms along the load axis for DLC-$P_{00}$ system after a 10 nN load has been applied but before sliding. (b) The right panel shows the density of carbon atoms in the $P_{00}$-DLC system after 200 ps of sliding. The red solid and blue dashed lines indicate the density of carbon atoms in the DLC counterface and $P_{00}$ film, respectively.

hydrogen termination to be larger than in the case of full counterface termination.

If DLC films are to be used as solid lubricants for micro- and nanoscale devices with moving parts, the tribology of self-mated surfaces must be understood. To that end, we have also used a hydrogen-terminated DLC counterface to examine the friction and wear of several amorphous carbon films [39, 4, 62]. Two such systems are shown in figures 13(a) and (b). Both films were attached to diamond (111) substrates and periodic boundary conditions were applied in the plane parallel to the sliding interface. The amount of hydrogen in the lower film was varied so that the effect of hydrogen content within the film on friction could be examined [39, 4]. One film had 0% hydrogen ($P_{00}$) and the other had 20% hydrogen ($P_{20}$). They were generated using the melt and quench technique [62] and their properties are summarized in table 1.

The sliding simulations were carried out by sliding the counterface (upper surface in figures 13(a) and (b)) at a constant velocity of approximately 1 Å ps$^{-1}$, while maintaining a constant load on the counterface. In addition to monitoring the normal and friction forces during the course of the simulation, the atomic coordination numbers were calculated so that chemical reactions could be monitored. Depending upon the nature of the film and the counterface, the number of chemical reactions that occur between the counterface and the film can be significant. For instance, figure 14 shows snapshots of the $P_{00}$ system at different points during the sliding. Due to the presence of unsaturated carbon in the $P_{00}$ film, the application of load has caused chemical reactions to occur between the tip and the sample prior to sliding. Once sliding begins, a dramatic increase in the number of interfilm chemical reactions occurred. This is apparent from examination of the lower panel of figure 14. The shearing action of the counterface has also caused bonds formed across the interface to be oriented in the direction of counterface motion. Interfilm chemical reactions that occur during sliding can make the analysis of the sliding simulation problematic. For example, to construct a friction versus load plot, the friction on the rigid layers of the counterface must be averaged over some time (or distance) interval. When reactions do not occur, the friction as a function of distance oscillates about some average value and the calculation of an average friction is straightforward. When the DLC counterface is in sliding

contact with the $P_{00}$ and $P_{20}$ films, interfilm reactions occur and the friction versus time data become irregular (figure 15(a)). In this case, the average friction value depends upon the time (or distance) interval over which the data are averaged. A time window after the period of increasing friction was chosen to calculate an average friction value. In this case, the time window between 166 and 200 ps was selected. Using this same window for all the simulations, the friction versus load data shown in figure 15(b) were obtained.

While tribochemical reactions are not uncommon when DLC is in sliding contact with DLC, many questions remain regarding the conditions that lead to tribochemistry, the composition of the transfer films formed, and the state of the counterface and films after the films have formed. MD simulations illuminate some of these questions. For example, the average friction of the $P_{20}$ film is lower than for the $P_{00}$ film at all the loads examined. The addition of hydrogen to the film caused a reduction in the number of interfilm carbon–carbon bonds formed by passivating the unsaturated carbon atoms on and near the surface of the $P_{20}$ film. Hydrogen in the substrate also affects the fate of the counterface during sliding. This is apparent from an examination of the average coordination number ($C_{ave}$) of the counterface as a function of time when it is in sliding contact with both the $P_{00}$ and $P_{20}$ films (figure 16). The average coordination number of the counterface decreases to a value close to 3 when in sliding contact with the $P_{00}$ film. Thus, most of the $sp^3$-hybridized carbon was converted to $sp^2$-hybridized carbon during sliding. In contrast, there is only a modest reduction in $C_{ave}$ when in sliding contact with the $P_{20}$ film.

The extent of chemical reactions that occur during sliding can also be quantified by calculating the thickness of the transfer film formed during sliding. Prior to sliding, all atoms in the system were assigned a tag to specify whether they belonged to the substrate film or counterface. During sliding, the locations of the substrate and counterface atoms were tracked using these tags. The transfer-layer thickness was estimated by determining the amount of mixing of substrate and counterface atoms. Figures 17(a) and (b) show the atomic density of the DLC-$P_{00}$ system as a function of distance along the loading axis. The red solid line indicates the density of the counterface carbon atoms, while the blue dashed line indicates the density of carbon atoms in the $P_{00}$ film. The lack of overlap between the blue and the red lines (figure 17(a)) is indicative of a lack of mixing of the counterface and $P_{00}$ atoms before sliding. Sliding for 200 ps caused considerable mixing of the counterface and the film atoms. The extent of crossover of the red and blue lines indicates the level of mixing of the substrate and counterface atoms (figure 17(b)). A transfer-layer thickness can be estimated by measuring the overlap of the lines and dividing by a two. Here, the assumption has been made that the equal parts of the transfer film will be transferred to the substrate and counterface upon separation. In general, the transfer film is thicker when the $P_{00}$ film is in sliding contact with the counterface compared to the $P_{20}$ film. The extraction of transfer film data from simulations may prove to be a particularly interesting value to obtain from the simulations because new experimental techniques have been developed to measure the thickness of these films [63, 64, 50].

## 6. Summary

Molecular dynamics simulations can provide unique insight into dynamic processes because the positions, time derivatives of position, and forces on all the atoms are known as a function of time. These quantities can be used to calculate many interesting quantities, some of which can be directly compared to experimental values, while others provide information not available from experiment. In this paper, we have reviewed some of the unique analysis techniques that we have used to examine indentation, compression, friction, and wear in hydrocarbon-containing systems. We have provided examples from our past, and current, work where these unique techniques have proven useful.

In this work, we have discussed our simulations that have examined the compression, indentation, and friction of SAMs. Quantification of order within these monolayers during the course of a simulation can be achieved by calculating quantities such as the tilt angle, methyl angle, structure factor, and number of gauche defects. Examples of the use of each of these quantities have been discussed. Our unique analysis of interfacial atomic contact forces has allowed for contribution of specific structural features within the SAMs to friction to be ascertained. An extensive discussion of the way in which these forces can be used to link structural differences to friction differences in SAMs composed of alkane chains with even and odd numbers of carbon atoms was presented.

The linking of friction differences to specific structural changes can be complicated by chemical reactions that occur during sliding. In these systems, because atoms can be transfered from the counterface to the substrate during sliding, the computation of atomic contact forces at the sliding interface can be problematic. In this case, analysis techniques, such as tracking the hybridization of the atoms, that are designed to illuminate the role of the chemical reactions should be undertaken. Our extensive simulations that have examined the friction of DLC versus DLC and the specialized analysis techniques that can be applied to these systems were discussed.

## Acknowledgments

JDS and Gao acknowledge support from The Air Force Office of Scientific Research (AFOSR) under contracts F1ATA07351G001 and F1ATA08018G001 (Extreme Friction MURI), respectively. PTM and MTK acknowledge support from the The Office of Naval Research (ONR) under contract N0001408WR20106. JAH acknowledges support from both ONR and AFOSR.

## References

[1] Harrison J A, Stuart S J and Brenner D W 1999 Atomic-scale simulation of tribological and related phenomena *Handbook of Micro/Nanotribology* 2nd edn, ed B Bhushan (Boca Raton, FL: CRC Press)

[2] Robbins M O and Müser M H 2001 Computer simulations of friction, lubrication, and wear *Modern Tribology Handbook* vol I, ed B Bhushan (Boca Raton, FL: CRC Press)

[3] Heo S J, Sinnott S B, Brenner D W and Harrison J A 2005 Computational modeling of nanometer-scale tribology *Nanotribology and Nanomechanics: an Introduction* ed B Bhushan (Heidelberg: Springer)
[4] Schall J D, Mikulski P, Chateauneuf G M, Gao G and Harrison J A 2007 Molecular dynamics simulations of tribology *Superlubricity* ed A Erdemir and J-M Martin (Amsterdam: Elsevier)
[5] Amar F and Berne B 1984 *J. Phys. Chem.* **88** 6720–7
[6] Smith E, Robbins M and Cieplak M 1996 *Phys. Rev.* B **54** 8252–60
[7] He G, Müser M and Robbins M O 1999 *Science* **284** 1650–62
[8] Müser M and Robbins M 2000 *Phys. Rev.* B **61** 2335–42
[9] Ryckaert J and Bellmans A 1978 *Discuss. Faraday Soc.* **66** 95–106
[10] Bird R B, Hassanger O, Armstrong R C and Curtiss C F 1977 *Dynamics of Polymeric Liquids* vol II (New York: Wiley)
[11] Daw M S and Baskes M I 1984 *Phys. Rev.* B **29** 6443–53
[12] Finnis M W and Sinclair J 1984 *Phil. Mag.* A **50** 45
[13] Foiles S, Baskes M and Daw M 1986 *Phys. Rev.* B **33** 7983–91
[14] Ercolessi F, Parrinello M and Tosatti E 1986 *Surf. Sci.* **177** 314–28
[15] Tersoff J 1986 *Phys. Rev. Lett.* **56** 632–5
[16] Tersoff J 1988 *Phys. Rev.* B **38** 9902–5
[17] Tersoff J 1988 *Phys. Rev.* B **37** 6991–7000
[18] Tersoff J 1989 *Phys. Rev.* B **39** 5566–8
[19] Brenner D W 1990 *Phys. Rev.* B **42** 9458–71
[20] Dyson A J and Smith P V 1996 *Surf. Sci.* **355** 140–50
[21] Sbraccia C, Silvestrelli P L and Ancilotto F 2002 *Surf. Sci.* **516** 147
[22] Beardmore K and Smith R 1996 *Phil. Mag.* A **74** 1439–66
[23] Brenner D W, Shenderova O A, Harrison J A, Stuart S J, Ni B and Sinnott S B 2002 *J. Phys.: Condens. Matter* **14** 783–802
[24] Gao G T, Van Workum K, Schall J D and Harrison J A 2006 *J. Phys.: Condens. Matter* **18** S1737
[25] Van Workum K, Gao G T, Schall J D and Harrison J A 2006 *J. Chem. Phys.* **125** 144506
[26] Ni B, Lee K H and Sinnott S B 2004 *J. Phys.: Condens. Matter* **16** 7261–75
[27] Schall J D, Gao G and Harrison J A 2008 *Phys. Rev.* B **77** 115209
[28] Che J, Cagin T and Goddard W A III 1999 *Theor. Chem. Acc.* **102** 346–54
[29] Stuart S J, Tutein A B and Harrison J A 2000 *J. Chem. Phys.* **112** 6472–86
[30] Harrison J A, Stuart S J and Tutein A B 2001 A new, reactive potential energy function to study the indentation and friction of $C_{13}$ n-alkane monolayers *ACS Symp. Series: Interfacial Properties on the Submicron Scale* vol 781, ed J Frommer and R M Overney (Washington, DC: American Chemical Society)
[31] Tutein A B, Stuart S J and Harrison J A 1999 *J. Phys. Chem.* B **103** 11357–65
[32] Tutein A B, Stuart S J and Harrison J A 2000 *Langmuir* **16** 291–6
[33] Mikulski P T and Harrison J A 2001 *J. Am. Chem. Soc.* **123** 6873–81
[34] Mikulski P T and Harrison J A 2001 *Tribol. Lett.* **10** 29–38
[35] Chateauneuf G M, Mikulski P T, Gao G T and Harrison J A 2004 *J. Phys. Chem.* B **108** 16626–35
[36] Mikulski P T, Gao G, Chateauneuf G M and Harrison J A 2005 *J. Chem. Phys.* **122** 024701-1–9
[37] Mikulski P T, Herman L A and Harrison J A 2005 *Langmuir* **21** 12197–206
[38] Harrison J A, Gao G T, Harrison R J, Chateauneuf G M and Mikulski P T 2004 The friction of model self-assembled monolayers *Encyclopedia of Nanoscience and Nanotechnology* vol 3, ed H S Nalwa (Los Angeles: American Scientific Publishers)
[39] Harrison J A, Gao G T, Schall J T, Knippenberg M T and Mikulski P 2008 *Phil. Trans. R. Soc.* A 1469–95
[40] Ulman A 1996 *Chem. Rev.* **96** 1533–54
[41] Nishi N, Hobara D, Yamamoto M and Kakiuchi T 2003 *J. Chem. Phys.* **118** 1904–11
[42] Knippenberg M T, Mikulski P T, Dunlap B I and Harrison J A 2008 in preparation
[43] Hoffmann H, Mayer U and Krischanitz A 1995 *Langmuir* **11** 1304–12
[44] Burns A R, Carpick R W, Sasaki D Y, Shelnutt J A and Haddad R 2001 *Tribol. Lett.* **10** 89–96
[45] Enkelmann V 1984 *Adv. Polym. Sci.* **63** 91–136
[46] Mowery M D, Kopta S, Ogletree D F, Salmeron M and Evans C 1999 *Langmuir* **15** 5118–22
[47] Cheadle E M, Batchelder D N, Evans S D, Zhang H L, Fukushima H, Miyashita S, Graupe M, Puck A, Shmakova O E, Colorado R Jr and Lee T R 2001 *Langmuir* **17** 6616–21
[48] Carpick R, Ogletree D and Salmeron M 1999 *J. Colloid Interface Sci.* **211** 395
[49] Erdemir A and Donnet C 2001 Tribology of diamond, diamond-like carbon, and related films *Modern Tribology Handbook* vol 2, ed B Bhushan (Boca Raton, FL: CRC Press LLC)
[50] Scharf T W and Singer I L 2003 *Thin Solid Films* **440** 138–44
[51] Grierson D S and Carpick R W 2007 *Nanotoday* **2** 12–21
[52] Grierson D, Sumant A, Konicek A, Abrecht M, Birrell J, Auciello O, Carlisle J, Scharf T, Dugger M, Gilbert P and Carpick R W 2007 *J. Vac. Sci. Technol.* 1700–5
[53] Sumant A, Krauss A, Gruen D, Auciello O, Erdemir A, Williams M, Artiles A and Adams W 2007 *Phys. Rev.* B **76** 235429
[54] Sumant A, Grierson D, Gerbi J, Birrell J, Lanke U, Auciello O, Carlisle J and Carpick R 2005 *Adv. Mater.* **17** 1039
[55] Houston M R, Howe R T, Komvopoulos K and Maboudian R 1995 *Mater. Res. Soc. Bull.* **383** 644–8
[56] Maboudian R, Ashurst W R and Carraro C 2002 *Tribol. Lett.* **12** 95–100
[57] Maboudian R and Howe R T 1997 *J. Vac. Sci. Technol.* B **15** 1–20
[58] Erdemir A, Fenski G R, Krauss A R, Gruen D M, McCauley T and Csencsits R T 1999 *Surf. Coat. Technol.* **120/121** 565–72
[59] Chromik R R, Winfrey A L, Lüning J, Nemanich R J and Wahl K J 2008 *Wear* **265** 477–89
[60] Larsen T, Moloni K, Flack F, Eriksson M, Lagally M G and Black C T 2002 *Appl. Phys. Lett.* **80** 1996
[61] Gao G T, Mikulski P T and Harrison J A 2002 *J. Am. Chem. Soc.* **124** 7202–9
[62] Gao G-T, Mikulski P T, Chateauneuf G M and Harrison J A 2003 *J. Phys. Chem.* B **107** 11082–90
[63] Scharf T W and Singer I L 2003 *Tribol. Lett.* **14** 2–8
[64] Scharf T W and Singer I L 2003 *Tribol. Lett.* **14** 137–45